Preparation and Properties of High Hardness Ultraviolet Curable Polyethylene Terephthalates Surface Coatings Modified with Octavinyl-Polyhedral Oligomeric Silsesquioxane

Tianmiao Kang, Liuyan Tang and Jinqing Qu *

School of Chemistry and Chemical Engineering, South China University of Technology, Guangzhou 510641, China; 15603059604@163.com (T.K.); demi0tong@foxmail.com (L.T.)
* Correspondence: cejqqu@scut.edu.cn

check for updates

Abstract: Using organic coatings helps to protect PET (polyethylene terephthalates) surfaces, improve surface hardness, scratch resistance, and solvent resistance, prolong the service life of PET film, and to expand their scope of applications. There were some disadvantages, including poor flexibility and impact resistance in high-hardness coatings; organic coatings should also be modified to improve the toughness. Herein, a UV (ultraviolet curing) curable high-hardness organic coating used in PET surface protection was prepared and modified with inorganic nanoparticles, such as OVPOSS (octavinyl-polyhedral oligomeric silsesquioxane). The effects of the categories of nanoparticles on the coating performance were studied. UV-Vis spectra (ultraviolet visible light spectra), FT-IR (Fourier transform infrared spectrometer), TGA (thermogravimetric analysis), DMA (dynamic-mechanical), SEM (field emission scanning electron microscope), and AFM (atomic force microscope) were used to characterize the properties of the coatings. The results showed that the addition of eight-vinyl POSS to the organic coating significantly increased its glass transition temperature (T_g) from 100 to 120 °C, improved its storage modulus from 167.6 to 258.9 MPa, and raised its impact resistance and flexibility. The SEM and AFM images displayed that the eight-vinyl POSS particles were dispersed homogeneously in the coating, arranged in an ordered network, and had good compatibility with organic components. The film displayed excellent properties, including 4 H of the pencil hardness, 100 g cm of impact resistance, excellent flexibility, and 90% of light transmittance, with the addition of 0.3 wt % OVPOSS. TGA analysis revealed that the coating had good thermal stability, with 5% weight loss temperature up to 335 °C.

Keywords: UV-curable; OVPOSS; PET optical film; thermal stability; storage modulus

1. Introduction

Polyethylene terephthalate (PET) film has been widely used in packaging decoration, screen protection, and optical grade mirror surface protection due to its excellent light transmission, heat resistance, toughness, and insulation [1]. However, PET film also easily deteriorate due to surface scratches, environmental stimulus of ultraviolet radiation, and chemicals, owing to its low surface hardness, weak abrasion resistance, and poor impact resistance. Using organic coatings to protect PET surfaces has helped to improve their performance, prolong the service life of PET film, and expand the applications of PET film in various fields [2]. However, present PET coatings have some disadvantages, including low film hardness (1–2 H), whereas high-hardness (4–6 H) PET coatings exhibit poor flexibility, impact resistance, and light transmittance, which should be improved.

Recent studies have reported that polymers modified with a small number of nanoparticles display some new functions based on the synergistic effect of nanomaterials and polymers. The reported nanoparticles include polyhedral oligomeric silsesquioxane (POSS) [3], nanosilica, nanoalumina, zirconia, nanotitania, JH-10 transparent glass powder, and so on [4,5]. Among them, octavinyl-polyhedral oligomeric silsesquioxane (OVPOSS) possesses unique cage structures (Si–O–Si inorganic skeleton and eight vinyl groups in the eight vertexes) [6–8], which enables OVPOSS to react with vinyl group monomers to produce high-strength and heat-resistant polymer hybrid materials. The cage structure also leads to the good compatibility of OVPOSS with polymer materials. Moreover, adding a small amount of OVPOSS could improve the surface hardness, heat resistance, impact resistance [9–13], and mechanical properties of the polymer. For example, using POSS carrying with different organic substituents (methacryl, glycidyl, and trisilanol phenyl) as the additive to the epoxy resin by directly mixing at loadings between 0.5 and 8 wt % significantly increased fracture toughness by an average of 130% and 400% [14], respectively. Cong and Cui [15] also reported that tetrafluoroethylene propylene elastomer octavinyl POSS (TFE/P-OVPOSS) composites containing various percentages of OVPOSS significantly enhanced the mechanical property and elevated the glass temperature of the composites. Zhou and Zhang [16] found that by physical blending or reactive blending, polypropylene (PP) with OVPOSS endowed the forming composites with good mechanical properties and thermal stability.

On the other hand, the use of solvent-free, high solid coatings with very low VOC (volatile organic compound) emissions permits to meet the increasingly stringent legal regulations in the industry. These coatings include UV-curable coatings that not only have low VOC contents, but also provide products of superior finished properties, such as gloss, durability, or abrasion resistance. Herein, a UV-curable high-hardness organic coating used in PET surface protection was prepared and modified with nanoparticles. The effects of the types and amounts of inorganic nanomaterials on coating performance were studied. The results indicated that the coated PET film displays excellent properties, including 4 H of the pencil hardness, good impact resistance, excellent flexibility, and high light transmittance, with the addition of 0.3 wt % OVPOSS [17,18].

2. Experimental Section

2.1. Material

Epoxy acrylate (EA, Zhuhai Changxing Chemical Materials, Zhuhai, China) and 6-functional aliphatic urethane acrylate (PUA, Wanhua Chemical, Beijing, China) were used as the main resins, pentaerythritol triacrylate (PETA) and 1,6-hexanediol diacrylate (HDDA, Jiangmen Sanmu Chemical, Jiangmen, China) were used as reactive diluents, linear thermoplastic polyacrylate (Garbo Chemical, Via Prati Nuovi, Italy) was used as a plasticizer, acetone (Yihua Chemical, Shanghai, China) and tetrahydrofuran (THF, Yihua Chemical, Shanghai, China) were used as solvents, and 125 μm PET film (Buddha DuPont Hongji Film Chemical, Foshan, China) was used as the substrate.

The inorganic component consisted of a transparent glass powder named JH-10, belonging to a quartz sand filler, whose model is TS010, and particle size is 2.5 μm, purchased from Jia Baoli Chemical (Shanghai, China). SiO_2 NPs, whose model is HL-150 and particle size is 20 nm, was prepared using the vapor deposition method. Al_2O_3 NPs, whose model is Aluna-100, and particle size is 13 nm, was prepared by AEROSIL similarly to the vapor deposition method. The two materials were both purchased from Guangzhou Top Billion Trade Chemical (Guangzhou, China). ZrO NPs (JC-R50, average particle sizes = 50 nm) and TiO_2 NPs (JC-T25, average particle sizes = 60 nm) were purchased from Shenzhen Jingdi Chemical (Shenzhen, China). Octavinyl polyhedral oligomeric silsesquioxane (OVPOSS, 98%) was prepared by Balingway Technology. 1-Hydroxycyclohexyl-phenyl-ketone (Irgacure184, Ciba Specialty Chemicals, Basel, Switzerland), and 2-Hydroxy-2-methyl-1-phenyl-1-prop-anone (Darocure1173, Shanghai Titan Technology, Shanghai, China) were used as photoinitiators.

2.2. Preparation of the Nanocomposite Films

The nanocomposite coatings were prepared by mixing the required amounts (100 g as the total mass of the coating system, using a percentage ratio shown in Tables 1–3) of organic resins (EA, PUA, HDDA, PETA, and 5 wt % linear thermoplastic polyacrylate), inorganic components (SiO_2 NPs, Al_2O_3 NPs, JH-10, ZrO NPs, TiO_2 NPs, or OVPOSS, as shown in Table 3), photoinitiators (3 wt % Darocure 1173 and 2 wt % Irgacure184), and solvents (13.3 g acetone and 10 g THF) to obtain dispersion with 30 wt % concentration. Finally, the dispersion was sonicated for 30 min to ensure the coating fineness was below 5 µm. The 125 µm PET film substrates were cleaned using acetone and deionized water three times to remove stains. Then, the films on the PET surface were prepared with an applicator—the thickness of the films was about 25 µm—and cured for 15 s under a mercury lamp (150–200 mJ/cm^2).

2.3. Characterization

Pencil hardness was characterized using a PPH-1 type tester according to the standardized pencil hardness test (GB/T 6739-86) [19]. Impact resistance was tested using a heavy impact tester based on the GB/T 1732-93 standardized test [20]. The standardized Crosshatch adhesion test (GB/T 9286-1998) [21] was used to test paint film adhesion. Flexibility was tested according to the GB/T 6742-86 standardized test [22]. The water resistance of the paint was carried out using the GB/T 1733-1993 method [23]. The chemical resistance properties, including acid, alkali, alcohol and salt, were detected by the GB/T 1763-1979 standardized test [24].

Ultraviolet visible light spectra (UV-Vis spectra) of the coating transmittance were recorded by the U-3010 spectrophotometer (Hitachi, Tokyo, Japan). The detected wavelength was 200–800 nm.

The change in the functional structure of OVPOSS before and after curing the UV coating was studied using a Fourier transform infrared spectrometer (FT-IR, Nicolet 5700, Nicolet company, New York, NY, USA). Infrared spectra were recorded using the KBr tableting method with a resolution of 4 cm^{-1} and scan times of 32.

Thermal gravity analysis (TG) was performed under nitrogen and air atmosphere on a TG 209 F3 Tarsus apparatus (Netzsch, Selb, Germany), from 25 to 600 °C, with a heating rate of 10 °C/min. The samples (about 5 mg) were placed in open alumina pans and fluxed with nitrogen or air (gas flow: 20 mL/min). Differential thermal gravity (DTG) was a differential curve of TG, used to measure the relationship between the rate of change in weight loss and the temperature of the sample under constant temperature rising conditions.

Dynamic–mechanical (DMA) analyses were performed using a DMA Q800 (TA Instruments, New Castle, DE, USA) in tensile configuration. The following experimental conditions were adopted: temperature range from 25 to 250 °C; heating rate of 5 °C/min; 1 Hz frequency; 0.05% of oscillation amplitude in strain-controlled mode; and sample with length × width × height: (30–50) mm × 8 mm × 2 mm. The storage modulus (E'), loss modulus (E''), and tan δ curve were recorded. T_g values were calculated from the peak value of tan δ curve.

A field emission scanning electron microscope (Hitachi uhr FE-SEM SU8200, Tokyo, Japan) was used to observe the dispersion morphology of different fillers in films. Three square millimeters of the cured film was adhered to the conductive adhesive. As the samples were not conductive, a gold film was plated on the surface of the film and placed in a vacuum chamber for electronic scanning.

An atomic force microscope (AFM, Nanoscope IIIa, Veeco Company, Plainview, NY, USA) was used to test the surface of hybrid films. The test mode was tapping mode and the resonance frequency was 1 Hz. The cantilever adjusted sum value used was greater than 2.5 and the vertical level signal was ±0.1. The cured film was stuck on the mica plate under the probe, and the instrument was adjusted to a proper position to carry out a scanning test of the sample surface topography.

3. Results and Discussion

3.1. Formula Optimization of UV-Curable Organic Coatings

The UV-curable coatings were prepared using different mass ratios of EA, PUA, HDDA, PETA, 3 wt % Darocure1173, and 2 wt % Irgacure184. 5 wt % linear thermoplastic polyacrylate was used as a plasticizer. The film hardness was tested and the results are listed in Table 1.

Table 1 illustrates that the film hardness increased with increasing the contents of EA, and all coatings exhibited high impact resistance, high chemical resistance, good optical transparency, and good adhesion on the PET surface. The optimum formula was Run 5.

Table 1. Compositions and hardness of UV-curable organic coatings.

Runs	EA (wt %)	PUA (wt %)	HDDA (wt %)	PETA (wt %)	Pencil Hardness
1	30	30	15	15	F
2	40	30	10	10	F
3	40	20	15	15	F
4	45	25	10	10	F
5	50	20	10	10	H

3.2. Effects of Nanoparticle Categories on the Harness of Hybrid Coatings

Using the composition ratio in Run 5, we investigated the effect of different inorganic nanoparticles on the pencil hardness of the coatings. Table 2 illustrates the effects of nanoparticle categories and additions on the film hardness. It was shown that the film hardness increased with the increase of nanoparticles addition until 0.5 wt %, then slightly decreased with the addition from 0.5–2.5 wt %. Finally, the film hardness increased with nanoparticle addition by more than 2.5 wt %. Nanoparticles were uniformly dispersed in the coating when their amounts were less than 0.5 wt %, so the films hardness were increased. When the content of nanoparticles was 0.5–2.5 wt %, an aggregation of nanoparticles occurred and caused inorganic–organic phase separation with the reduction of film hardness. When the content of nanoparticles exceeded 2.5 wt %, the nanoparticles reunited on the surface coating and the hardness of air-contacted surfaces increased with the decrease of light transmission. Moreover, Table 3 shows that the film harnesses with SiO_2 NPs, JH-10 and OVPOSS were higher than those with the other nanoparticles, and the OVPOSS displayed the best hardness enhancement effect: The harness of the OVPOSS hybrid coating was the highest and reached 4 H with a 0.3 wt % addition.

Table 2. Fillers composition and hardness of composite coatings.

Nanoparticles	Addition Amount of Nanoparticles (wt %)								
	0.10	0.20	0.30	0.40	0.50	1.50	2.50	3.50	4.50
JH-10	2 H	2 H	3 H	3 H	3 H	2 H	3 H	2 H	3 H
SiO_2	2 H	2 H	3 H	3 H	3 H	2 H	4 H	4 H	4 H
ZrO	2 B	2 B	F	F	F	H	3 H	H	2 H
TiO_2	F	F	F	F	F	3 H	3 H	3 H	3 H
Al_2O_3	F	F	3 H	3 H	3 H	3 H	3 H	3 H	3 H
OVPOSS	2 H	3 H	4 H	3 H	3 H	3 H	2 H	2 H	2 H

According to Table 2, generally, the pencil hardness of the coatings with 0.3% inorganic nanoparticles was higher than that with other content. Therefore, we studied the other mechanical properties of the coatings with 0.3 wt % nanoparticles.

Table 3 lists the film properties, including hardness, impact resistance, and flexibility, modified by 0.3 wt % nanoparticles. It was observed that the hardness of the composite coatings was higher than that of the pure organic coating. All the coatings had good light transmittance and excellent water and

chemical resistance. Although it had relatively good flexibility, Film 4 had a poor adhesive and impact resistance. The hardness of Film 5 was the highest up to 4 H, and its impact resistance was also the best up to 102 g cm. The probable reason for the excellent performance of Film 5 was that OVPOSS reacted with acrylate monomer and displayed good compatibility with the organic phase.

Table 3. The film properties modified by 0.3 wt % nanoparticles.

Samples	Nano Particles	Pencil Hardness	Impact Resistance (cm)	Adhesion (Level)	Flexibility (mm)
Film 1	0	H	80	0	2
Film 2	SiO_2	3 H	40	0	2
Film 3	JH-10	3 H	40	0	2
Film 4	Al_2O_3	3 H	5	2	4
Film 5	OVPOSS	4 H	102	0	2

3.3. The Transmittance of Composite Coating

The PET surface coating required high transmittance up to 90%. The transmittance of the composite coatings is shown in Figure 1 with different fillers in UV-Vis wavelength ranging from 200 to 800 nm.
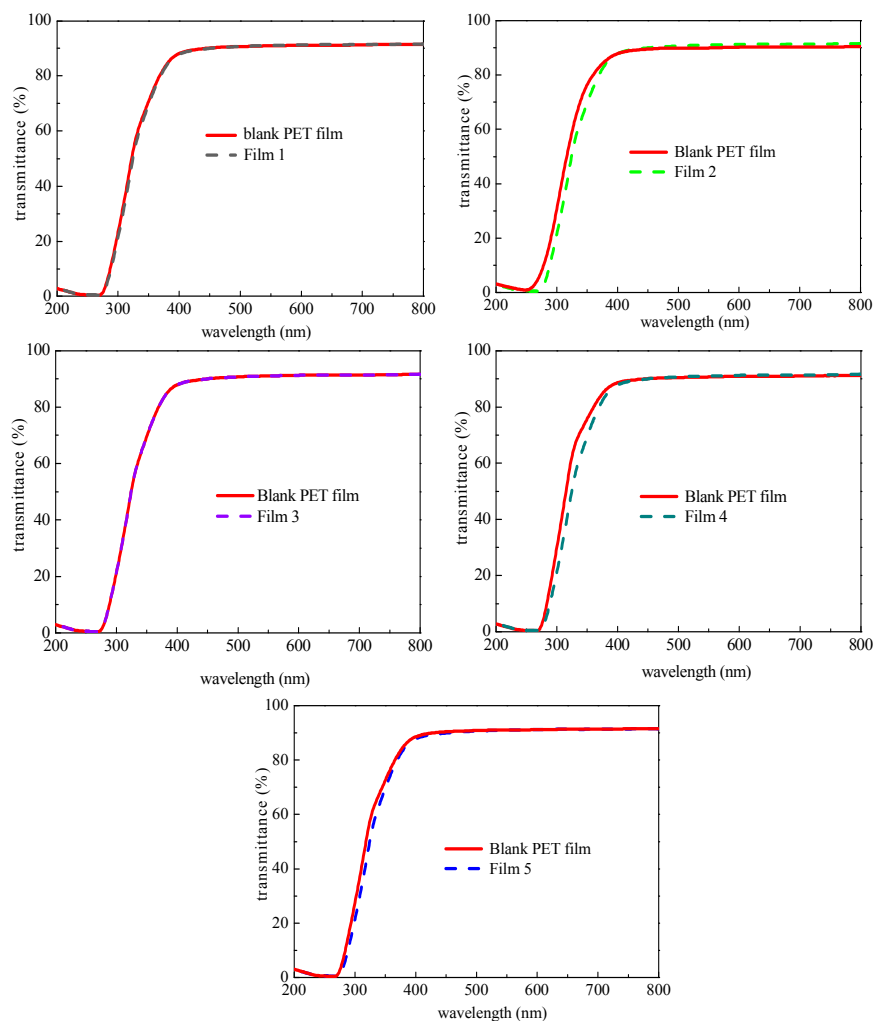

Figure 1. Effect of different nanoparticles on the transmittance of UV-cured films.

Figure 1 shows that the transmittance of all the coatings was up to 90%. In the wavelength range from 250 nm to 400 nm, the transmittance of Films 1 and 3 was consistent with that of the blank PET film, whereas the transmittance of Films 2, 4, and 5 was slightly lower than that of the blank PET film. However, in the visible light region (400–800 nm), the transmittance of the composite coatings containing SiO_2 NPs, Al_2O_3 NPs, and OVPOSS become lower than that of the blank PET film. That is because the reunion of SiO_2 NPs, and Al_2O_3 NPs hindered the further progress of the curing, causing numerous unsaturated double bonds to remain, resulting in the absorption of light in this wavelength region.

Interestingly, the addition of OVPOSS into the coating did not significantly affect the light absorption of PET film in the same wavelength region. OVPOSS participated in the crosslinking reaction, which increased the degree of crosslinking. For this reason, although the reunion of OVPOSS also blocked the curing progress, the light transmittance of this coating was similar to that of the blank PET film.

3.4. The Fourier Transform IR (FTIR) Spectroscopy of Composite Coating

To analyze whether the OVPOSS participates in the free radical polymerization, the comparison of infrared spectra before and after curing the OVPOSS hybrid coating is shown in Figure 2.

In Figure 2, the absorption peak at 1123 cm^{-1} was the asymmetric stretching vibration of Si–O–Si in OVPOSS. The peak at 1413 cm^{-1}, 992 cm^{-1}, and 1267 cm^{-1} was the in-plane and outward bending vibration absorption peak of the carbon–hydrogen bond of Si–CH=CH$_2$. The C=C absorption peak at 2985 cm^{-1} and 1604 cm^{-1} in the infrared curves of OVPOSS was obvious, but decreased in the infrared curves of the OVPOSS hybrid coating before and after curing, indicating the successful polymerization under the action of the photoinitiator. The completion of the Si–O bond reaction was evidenced by the absence of the symmetric denaturing vibration of Si–O skeleton at 589 cm^{-1}, indicating that the Si–O bond reaction was complete in the infrared curves of the OVPOSS hybrid coating before and after curing. The vibration absorption peak of C–H on the vinyl group at 2985 cm^{-1} decreased; it could be that the transfer to the macromolecular chain during the radical polymerization resulted in a crosslinked polymer forming a macromolecular polymer containing a Si–O–Si network structure.
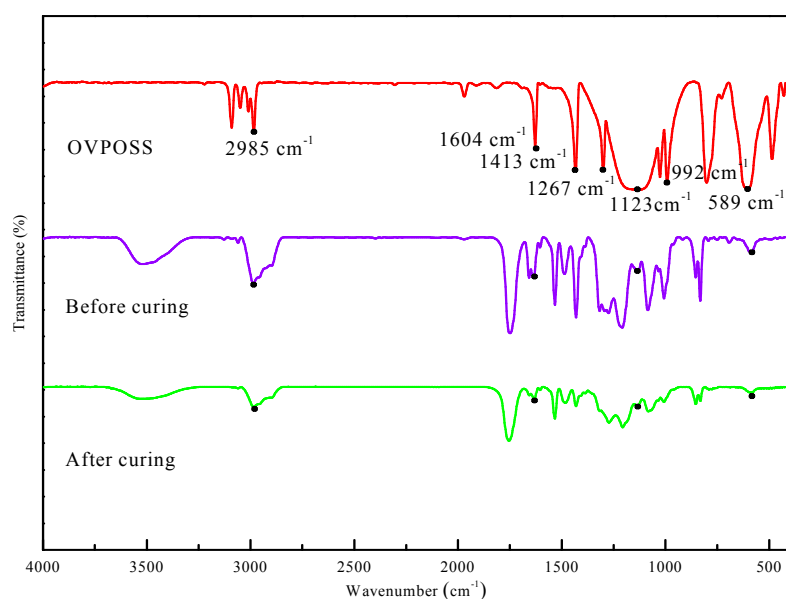

Figure 2. The infrared spectra of octavinyl polyhedral oligomeric silsesquioxane (OVPOSS) hybrid coating before and after curing.

3.5. Thermal Characterization

Figure 3 shows the TG (thermal gravity analysis) and DTG (differential thermal gravity, differential curve of TG) curves of the pure organic and composite coatings listed in Table 4. $T_{-5\%}$ (temperature at which 5% weight loss occurs), $T_{-50\%}$ (temperature at which 50% weight loss occurs), $T_{\max}$ (temperature at which maximum weight loss rate was achieved), $R_{\max}$ (maximum decomposition rate), and residue rate at 600 °C were evaluated.
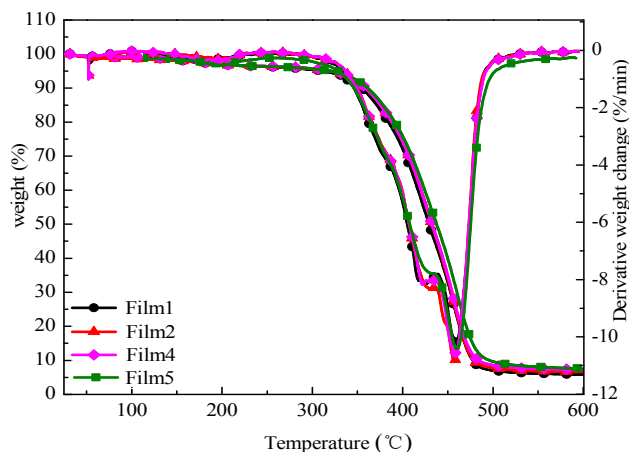

Figure 3. Thermal gravity (TG) and differential TG (DTG) curves of pure organic and composite coatings.

Table 4. Thermogravimetric data of pure organic and composite films.

Runs	$T_{-5\%}$ (°C)	$T_{-50\%}$ (°C)	$T_{\max}$ (°C)	$R_{\max}$ (%/min)	Residue Rate at 600 °C (%)
Film 1	315.5	429.6	457.3	10.19	5.868
Film 2	319.2	431.7	455.5	10.85	6.591
Film 4	320.2	433.5	457.2	10.56	7.446
Film 5	335.2	437.9	459.6	10.22	8.265

Figure 3 and Table 4 demonstrate that the thermal stability of the hybrid coatings was improved by the addition of nanoparticles. The thermal stability of the hybrid coating modified by OVPOSS was the best among all the prepared hybrid coatings. One apparent evidence is that, with OVPOSS, the $T_{-5\%}$ of the film increased from 315.5 to 335.2 °C. We believe that the high thermal stability of OVPOSS modified hybrid coating is attributed to the unique cage structure of OVPOSS. OVPOSS contained a thermal stable Si–O–Si inorganic skeleton and eight vinyl groups that increased the crosslinking density of the hybrid coating, resulting in the increase of the thermal decomposition temperature.

3.6. Dynamic–Mechanical Characterization

Figure 4 illustrates the storage modulus (E'), loss modulus (E''), and tan δ curve of the hybrid coatings modified with different nanoparticles, and detailed information is listed in Table 5.

With the addition of SiO$_2$ NPs, JH-10, and OVPOSS, the T_{g} of the films increased to 125.6 °C, 125.2 °C, and 127.6 °C, respectively. The storage modulus E' improved in the rubbery plateau to 185.5, 254.3, and 258.9 MPa, respectively. The increase of T_{g} and E' is owing to the dispersion or aggregation of inorganic materials in the polymer, which limited the free movement of the polymer chain [25,26]. The T_{g} and E' of Film 5 were the highest because the presence of OVPOSS intensifies the dampening effect at temperatures up to T_{g}, as revealed by the larger values of E'' in this region. Therefore, the hybrid coating required more energy to promote the cured completion. This makes it difficult for the hybrid film to transit from the glassy state to the rubbery state, eventually leading to an increase in T_{g} [27].
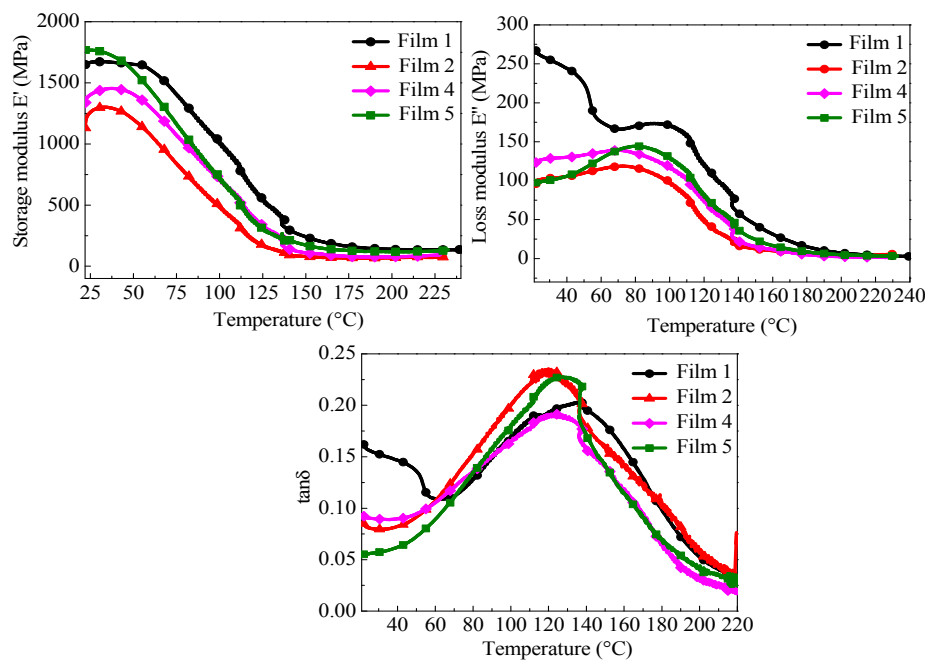
Figure 4. The effect of different inorganic materials on the storage modulus (E'), loss modulus (E''), and tan δ curve of the coatings.

Table 5. The data of the UV-cured organic and hybrid coating obtained from dynamic–mechanical analysis (DMA).

Runs	E' (MPa)	E'' (MPa)	tan δ	T_g (°C)
Film 1	167.6	111.4	0.189	122.9
Film 2	185.5	38.3	0.204	125.6
Film 4	254.3	50.8	0.202	125.2
Film 5	258.9	58.2	0.228	127.6

3.7. SEM Characterization

The SEM images of hybrid film are shown in Figure 5. Figure 5A shows the UV-curable organic film without any nanoparticles. The crystal structures attributed to the hard segment macrophase from EA resins can clearly be observed. Figure 5B,C displays that the SiO_2 NPs and JH-10 were mostly presented as aggregates on the coating surface. The generation of the large nanoparticle aggregates was promoted by the hydrogen bonds between the hydroxyl group on the SiO_2 NPs surface. The JH-10 glass powder was silica and did not participate in the photocuring reaction, which makes the coating experience local stress; impact resistance was poor, so the coating was easy to break, then peel off. These aggregates indicated the uneven dispersion of nanoparticles and were to blame for the decrease in the impact resistance of the coatings. As shown in Figure 5D, OVPOSS particles were distributed in the coating in an orderly stacking manner [28]. This manner was also supported by the cage structure of OVPOSS and was beneficial to the performance of the hybrid coatings.
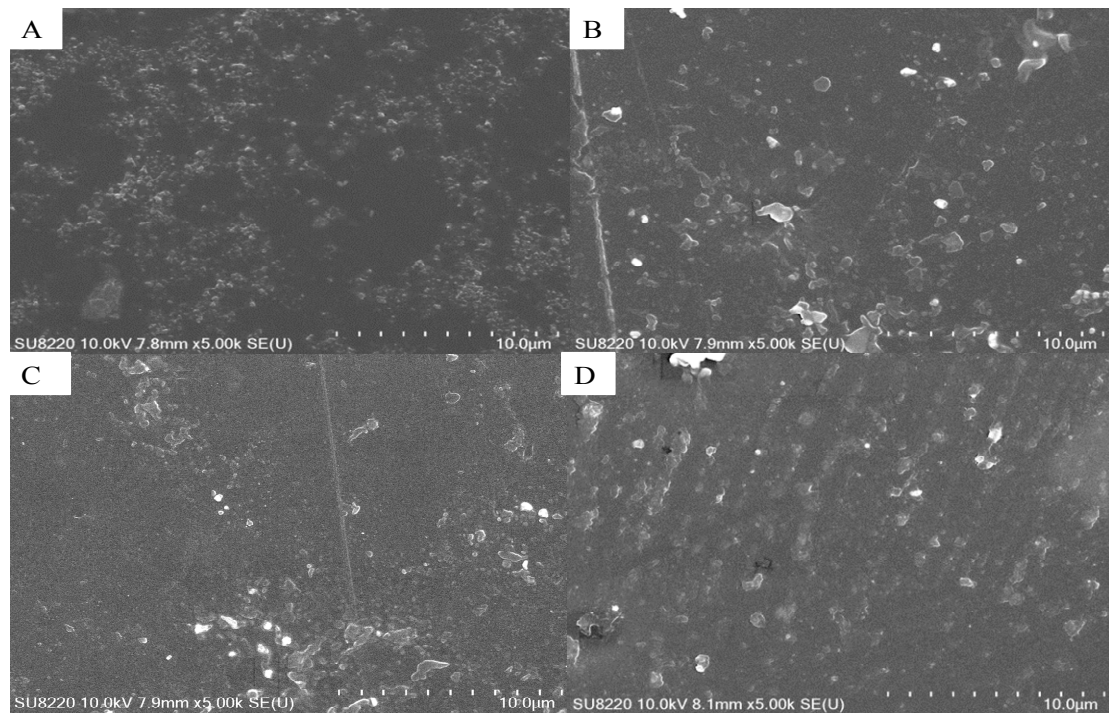
Figure 5. The SEM images of hybrid films: (**A**) Film 1; (**B**) Film 2; (**C**) Film 4; (**D**) Film 5.

3.8. AFM Characterization

The surface morphologies of the organic and doped coatings were obtained by an AFM (Figures 6 and 7 and Table 6). In Table 6, R_a, RMS, R_z, and R_z Count represented average surface roughness, root mean square roughness, 10 points average roughness, and counting points, respectively. It can be inferred from Table 6 that the roughness of Film 1 without inorganic particles was the smallest and the surface of the coating was the smoothest, with R_a = 0.843 nm and RMS = 1.148 nm. The addition of SiO_2 NPs, JH-10, and OVPOSS increased the roughness of the coatings. R_a of Film 5 approached 1.370 nm, but it did not affect the smoothness of the coating surface. Figures 6 and 7 demonstrate that there was a distinct two-phase structure on the coating surfaces. The low concave portion corresponded to the organic phase, while the white microregion of the convex portion corresponded to the hardened portion of the inorganic phase. It was obvious that the light-colored convex portions of Figure 6B,C were distributed in a disorderly disordered or aggregated manner on film surface, because SiO_2 NPs contained a lot of –OH and JH-10 had poor compatibility with the organic phases. According to Figure 6D, the particle density of Film 5 was higher than that of the other coatings and the OVPOSS particles were uniformly dispersed in the film in an orderly manner. Film 5 also had a large specific interface with organic polymers and strong binding force, which enhanced the hardness, scratch resistance, and impact resistance of the organic material.
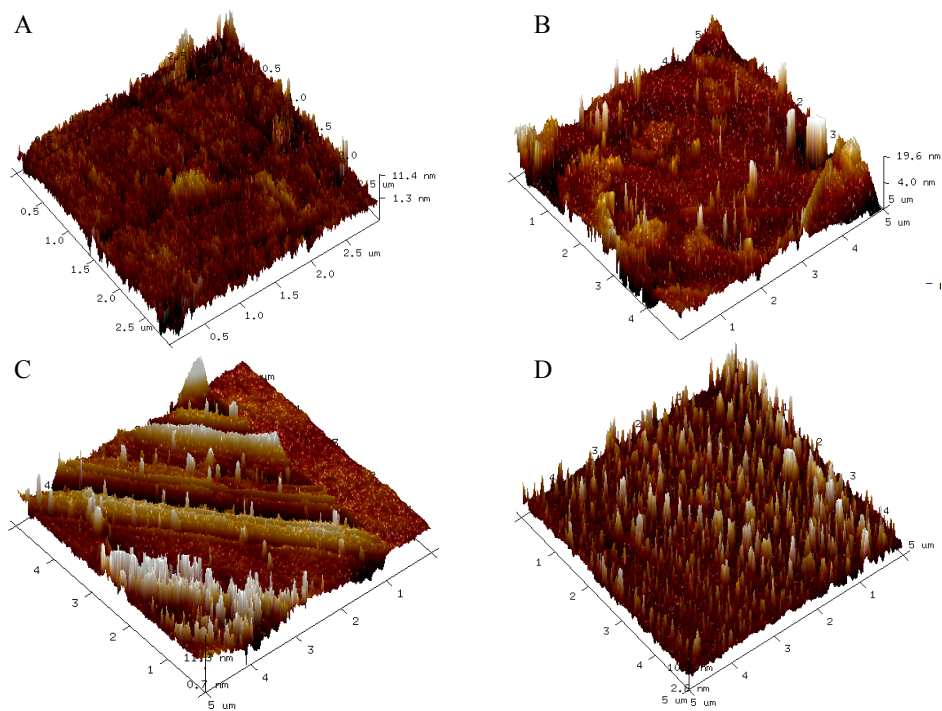
Figure 6. Atomic force microscope (AFM) 3D images of organic and composite coatings: (**A**) Film 1; (**B**) Film 2; (**C**) Film 4; (**D**) Film 5.
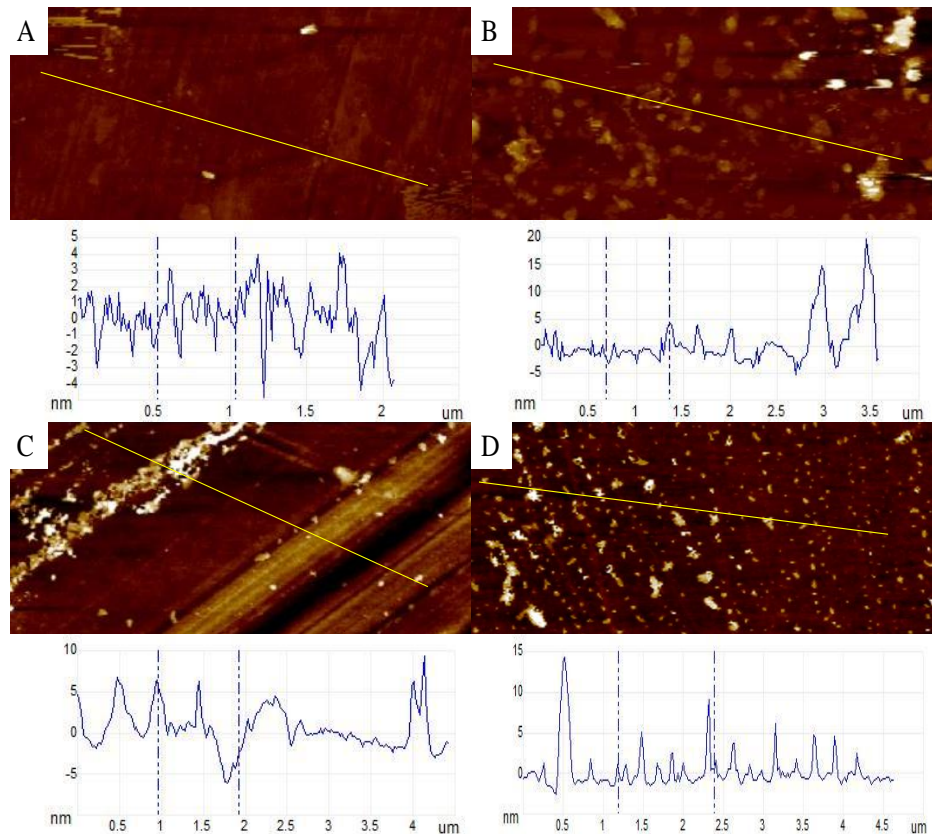

Figure 7. AFM 2D images and their corresponding height profiles of organic and composite coatings: (**A**) Film 1; (**B**) Film 2; (**C**) Film 4; (**D**) Film 5.

Table 6. Roughness statistics of organic and composite coating surfaces.

Runs	R_a (nm)	RMS (nm)	R_z (nm)	R_z Count
Film 1	0.843	1.148	2.551	10
Film 2	1.072	1.424	2.843	10
Film 4	2.279	2.606	3.845	10
Film 5	1.370	3.877	3.804	10

4. Properties Comparison

Table 7 lists the performances of unmodified organic coating and the OVPOSS modified hybrid coating on the surface of PET.

Table 7. Performance of unmodified and OVPOSS modified film.

Coating Performance	Unmodified Film	OVPOSS Modified Film
Pencil hardness	H	4 H
Adhesion (level)	0	0
Impact resistance (g cm)	80	102
Flexibility (mm)	2	2
Water resistance	good [a]	good [c]
Chemical resistance	good [b]	good [d]
Transmittance (%)	$\geq$90	$\geq$90
T_g (°C)	100	120
5% loss weight Tem. (°C)	315.5	335.2
600 °C residual rate (%)	5.87	8.27
Storage modulus (MPa)	167.6	258.9

[a,c]: "good" means that film is not white, not wrinkled, unbroken through 24 h water immersion; [b,d]: "good" means that film is not white, undamaged, undropped by dropping 5% NaCl, 5% NaHCO$_3$, 5% acetic acid, 10% alcoholic through 24 h at room temperature.

Table 7 discloses that the hybrid coating modified with 0.3 wt % OVPOSS displayed a better performance than the UV-curable organic coating. The hybrid coating exhibited 4 H of the hardness and good flexibility, and could be used in the PET surface protection.

5. Conclusions

A UV-curable high-hardness organic coating used in PET surface protection was prepared and modified with inorganic nanoparticles, such as OVPOSS. The effects of the categories and amounts of the nanoparticles on the coating performance were studied. It was found that the composite coatings modified by 0.3 wt % OVPOSS had high hardness (4 H), excellent impact resistance (102 g cm), good adhesion, and high flexibility. In addition, its transmittance was more than 90%. The hybrid coating modified by 0.3 wt % OVPOSS also had a good thermal stability. Its 5% weight loss temperature reached 335.2 °C and its storage modulus (E') was improved up to 258.9 MPa. The AFM images showed the OVPOSS particles dispersed evenly in the coating, arranged in an ordered network, and had good compatibility with organic components. The coatings not only effectively improved the surface properties of PET films through UV technological preparation, but also brought the long-term and extensive reference to the preparation of optical coatings through a simple and controllable method.

Author Contributions: Methodology, T.K. and J.Q.; Investigation, T.K.; Formal Analysis, T.K.; Writing–Original Draft Preparation, T.K.; Writing–Review & Editing, L.T., J.Q.; Supervision, L.T., J.Q.; Investigation, L.T., J.Q.; Validation, L.T., J.Q.; Visualization, L.T.

Conflicts of Interest: The authors declare no conflict of interest.

References

1. Agnieszka, E.W.; Małgorzata, J.; Agata, G.; Marta, W. Interfacial properties of PET and PET/starch polymers developed by air plasma processing. *Colloids Surf. A Physicochem. Eng. Asp.* **2017**, *532*, 323–331.
2. Gotoh, K.; Kobayashi, Y.; Yasukawa, A.; Ishigami, Y. Surface modification of PET films by atmospheric pressure plasma exposure with three reactive gas sources. *Colloid Polym. Sci.* **2012**, *290*, 1005–1014. [CrossRef]
3. Zhang, K.; Qiu, Z. Influence of low octavinyl-polyhedral oligomeric silsesquioxanes loadings on the crystallization kinetics and morphology of poly(ethylene suberate). *Thermochim. Acta* **2017**, *655*, 94–100. [CrossRef]
4. Ng, Y.-H.; Tay, S.-W.; Liang, H. Donut-like hybrid latex comprising discrete thermoplastic lobe and thermosetting shell. *Polymer* **2016**, *98*, 252–262. [CrossRef]
5. Liao, W.; Huang, X.; Ye, L.; Lan, S.; Fan, H. Synthesis of composite latexes of polyhedral oligomeric silsesquioxane and fluorine containing poly(styrene-acrylate by emulsion copolymerization. *J. Appl. Polym. Sci.* **2016**, *133*, 43455. [CrossRef]
6. Zhang, C.; Bai, X.; Lian, X.; Dou, Y.; Liu, H. Study on morphology and mechanical properties of PMMA-based nanocomposites containing POSS molecules or functionalized SiO_2 particles. *High Perform. Polym.* **2011**, *23*, 468–476. [CrossRef]
7. Amerio, E.; Sangermano, M.; Colucci, G.; Malucelli, G.; Messori, M. UV curing of organic–inorganic hybrid coatings containing polyhedral oligomeric silsesquioxane blocks. *Macromol. Mater. Eng.* **2010**, *293*, 700–707. [CrossRef]
8. Akiyama, H.; Ohtani, N. Fabrication and optical characterization of organic–inorganic hybrid films using ultraviolet-curable silsesquioxanes. *Jpn. J. Appl. Phys.* **2014**, *53*, 02BC18. [CrossRef]
9. Lee, A.S.; Jo, Y.Y.; Jeon, H.; Choi, S.S.; Baek, K.Y.; Hwang, S.S. Mechanical properties of thiol-ene UV-curable thermoplastic poly-silsesquioxanes. *Polymer* **2015**, *68*, 140–146. [CrossRef]
10. Jankauskaitė, V.; Lazauskas, A.; Griškonis, E.; Lisauskaitė, A.; Žukienė, K. UV-curable aliphatic silicone acrylate organic–inorganic hybrid coatings with antibacterial activity. *Molecules* **2017**, *22*, 964. [CrossRef] [PubMed]
11. Carosio, F.; Di Pierro, A.; Alongi, J.; Saracco, G. Controlling the melt dripping of polyester fabrics by tuning the ionic strength of polyhedral oligomeric silsesquioxane and sodium montmorillonite coatings assembled through layer by layer. *J. Colloid Interface Sci.* **2018**, *510*, 142–151. [CrossRef] [PubMed]
12. Devaux, E.; Rochery, M.; Bourbigot, S. Polyurethane/clay and polyurethane/POSS nanocomposites as flame retarded coating for polyester and cotton fabrics. *Fire Mater.* **2002**, *26*, 149–154. [CrossRef]
13. Malucelli, G.; Fioravanti, A.; Francioso, L.; De Pascali, C.; Signore, M.A.; Carotta, M.C.; Bonanno, A.; Duraccio, D. Preparation and characterization of UV-cured composite films containing ZnO nanostructures: Effect of filler geometric features on piezoelectric response. *Prog. Org. Coat.* **2017**, *109*, 45–54. [CrossRef]
14. Mishra, K.; Pandey, G.; Singh, R.P. Enhancing the mechanical properties of an epoxy resin using polyhedral oligomeric silsesquioxane (POSS) as nano-reinforcement. *Polym. Test.* **2017**, *62*, 210–218. [CrossRef]
15. Cong, C.; Cui, C.; Meng, X.; Zhou, Q. Structure and property of tetrafluoroethylene-propylene elastomer-OVPOSS composites. *J. Appl. Polym. Sci.* **2013**, *130*, 1281–1288.
16. Zhou, Z.; Zhang, Y.; Zeng, Z.; Zhang, Y. Properties of POSS-filled polypropylene: Comparison of physical blending and reactive blending. *J. Appl. Polym. Sci.* **2008**, *110*, 3745–3751. [CrossRef]
17. Takeuchi, H.; Konno, T.; Mori, H. Synthesis of multifunctional silsesquioxane nanoparticles with hydroxyl and polymerizable groups for UV-curable hybrid coating. *React. Funct. Polym.* **2017**, *115*, 43–52. [CrossRef]
18. Florea, N.M.; Lungu, A.; Badica, P.; Craciun, L.; Enculescu, M.; Ghita, D.G.; Ionescu, C.; Zgirian, R.G.; Iovu, H. Novel nanocomposites based on epoxy resin/epoxy-functionalized polydimethylsiloxane reinforced with POSS. *Compos. Part B Eng.* **2015**, *75*, 226–234. [CrossRef]
19. *GB/T 6739-86 Determination of Film Hardness by Pencil Test*; National Technical Supervision Bureau: Beijing, China, 1986.
20. *GB/T 1732-93 Determination of Impact Resistance of Film*; National Technical Supervision Bureau: Beijing, China, 1993.

21. *GB/T 9286-1998 Paints and Varnishes-Cross Cut Test for Films*; National Technical Supervision Bureau: Beijing, China, 1998.
22. *GB/T 6742-86 Bend Test for Coating (Cylindrical Mandrel)*; National Bureau of Standards: Beijing, China, 1986.
23. *GB/T 1733-1993 Determination of Resistance to Water of Films*; National Technical Supervision Bureau: Beijing, China, 1993.
24. *GB/T 1763-1979 Methods of Test for Chemical Resistance of Paint Films*; National Standards Administration: Beijing, China, 1979.
25. Zhao, Y.; Schiraldi, D.A. Thermal and mechanical properties of polyhedral oligomeric silsesquioxane (POSS)/polycarbonate composites. *Polymer* **2005**, *46*, 11640–11647.
26. Chiu, Y.-C.; Chou, I.-C.; Tsai, H.-C.; Riang, L.; Ma, C.-C.M. Morphology, thermal and mechanical properties of the polyhedral oligomeric silsesquioxane side-chain epoxy hybrid material. *J. Appl. Polym. Sci.* **2010**, *118*, 3723–3732. [CrossRef]
27. Eftekhari-Sis, B.; Rahimkhoei, V.; Akbari, A.; Araghi, H.Y. Cubic polyhedral oligomeric silsesquioxane nano-cross-linked hybrid hydrogels: Synthesis, characterization, swelling and dye adsorption properties. *React. Funct. Polym.* **2018**, *128*, 47–57. [CrossRef]
28. Blanco, I.; Abate, L.; Bottino, F.A. Mono substituted octaphenyl POSSs: The effects of substituents on thermal properties and solubility. *Thermochim. Acta* **2017**, *655*, 117–123. [CrossRef]